Journal of Pharmaceutical Analysis 15 (2025) 101199

Contents lists available at ScienceDirect

Journal of Pharmaceutical Analysis

journal homepage: www.elsevier.com/locate/jpa

Original article

Tailoring a traditional Chinese medicine prescription for complex diseases: A novel multi-targets-directed gradient weighting strategy

Zhe Yu [a, 1], Teng Li [a, 1], Zhi Zheng [b, c], Xiya Yang [a], Xin Guo [a, d], Xindi Zhang [a], Haoying Jiang [a], Lin Zhu [a], Bo Yang [a], Yang Wang [a], Jiekun Luo [a], Xueping Yang [a], Tao Tang [e, f, g, **], En Hu [e, f, g, *]

[a] Institute of Integrative Medicine, Department of Integrated Traditional Chinese and Western Medicine, Xiangya Hospital, Central South University, Changsha, 410008, China
[b] Department of Neurology, Xiangya Hospital, Central South University, Jiangxi (National Regional Center for Neurological Diseases), Nanchang, 330038, China
[c] Jiangxi Provincial People's Hospital, The First Affiliated Hospital of Nanchang Medical College, Nanchang, 330038, China
[d] The First Affiliated Hospital, Children's Medical Centre, Hengyang Medical School, University of South China, Hengyang, Hunan, 421001, China
[e] Institute of Integrative Medicine, Department of Integrated Traditional Chinese and Western Medicine, Xiangya Hospital, Central South University, Jiangxi (National Regional Center for Neurological Diseases), Nanchang, 330038, China
[f] NATCM Key Laboratory of TCM Gan, Xiangya Hospital, Central South University, Changsha, 410008, China
[g] National Clinical Research Center for Geriatric Disorders, Xiangya Hospital, Central South University, Changsha, 410008, China

ARTICLE INFO

Article history:
Received 10 July 2024
Received in revised form
27 December 2024
Accepted 12 January 2025
Available online 16 January 2025

Keywords:
Traditional Chinese medicine
Prescription formulation
Gradient weighting strategy
Multiple targets
Intracerebral hemorrhage

ABSTRACT

Traditional Chinese medicine (TCM) exerts integrative effects on complex diseases owing to the characteristics of multiple components with multiple targets. However, the syndrome-based system of diagnosis and treatment in TCM can easily lead to bias because of varying medication preferences among physicians, which has been a major challenge in the global acceptance and application of TCM. Therefore, a standardized TCM prescription system needs to be explored to promote its clinical application. In this study, we first developed a gradient weighted disease-target-herbal ingredient-herb network to aid TCM formulation. We tested its efficacy against intracerebral hemorrhage (ICH). First, the top 100 ICH targets in the GeneCards database were screened according to their relevance scores. Then, SymMap and Traditional Chinese Medicine Systems Pharmacology (TCMSP) databases were applied to find out the target-related ingredients and ingredient-containing herbs, respectively. The relevance of the resulting ingredients and herbs to ICH was determined by adding the relevance scores of the corresponding targets. The top five ICH therapeutic herbs were combined to form a tailored TCM prescriptions. The absorbed components in the serum were detected. In a mouse model of ICH, the new prescription exerted multifaceted effects, including improved neurological function, as well as attenuated neuronal damage, cell apoptosis, vascular leakage, and neuroinflammation. These effects matched well with the core pathological changes in ICH. The multi-targets-directed gradient-weighting strategy presents a promising avenue for tailoring precise, multipronged, unbiased, and standardized TCM prescriptions for complex diseases. This study provides a paradigm for advanced achievements-driven modern innovation in TCM concepts.

* Corresponding author. Institute of Integrative Medicine, Department of Integrated Traditional Chinese and Western Medicine, Xiangya Hospital, Central South University, Jiangxi (National Regional Center for Neurological Diseases), Nanchang, 330038, China.
** Corresponding author. Institute of Integrative Medicine, Department of Integrated Traditional Chinese and Western Medicine, Xiangya Hospital, Central South University, Jiangxi (National Regional Center for Neurological Diseases), Nanchang, 330038, China.
E-mail addresses: znxyhe@csu.edu.cn (E. Hu), tangtaotay@csu.edu.cn (T. Tang).
Peer review under responsibility of Xi'an Jiaotong University.
[1] Both authors contributed equally to this work.

https://doi.org/10.1016/j.jpha.2025.101199

1. Introduction

Most diseases are complex and are accompanied by a network interplay of multifactorial pathophysiological dynamics [1]. Therefore, a multi-target therapy is needed for intractable diseases, such as cancers and central nervous system diseases [2,3].

Traditional Chinese medicine (TCM) is a widely applied, multi-component, and multi-target therapy that achieves integrated and systemic efficacy in complex diseases. TCM prescriptions are composed of functionally synergistic or complementary natural medicines based on the records of ancient physicians or the TCM theory. However, TCM formulation processes empirically rely on symptom-based syndrome differentiation. As a result, the composition, doses, and efficacy of TCM prescriptions largely depend on the personal experience and preferences of medical practitioners, which can be optimized. More importantly, owing to the lack of a certain standard, formulating an effective TCM prescription is difficult for most physicians without sufficient systemic TCM knowledge. This has been a major challenge for the global acceptance and application of TMC. Recently, a strategy that integrates extensive ancient prescriptions and famous physician cases has been widely used in TCM optimization. By leveraging big data, this approach can be used to formulate new and effective prescriptions by combining the core herbs [4–6]. However, owing to the selective bias of herbs in the source data, this approach may further amplify the contributions of herbs in commonly used classical formulas. Therefore, a more quantitative, evidence-based, and easy-to-use formulation strategy is required to improve the standardization and curative power of TCM to promote its modernization and globalization.

Modern research has achieved substantial advancements in understanding the relationships between diseases, molecular targets, herbal ingredients, and herbs. However, in current TCM practice, network relations are applied in an overly mechanical and simple manner, where they merely serve to explain the mechanisms of the actions of TCM using a network pharmacology approach [2,7–9]. Nevertheless, they are rarely used to create, optimize, or standardize TCM prescriptions. In contemporary drug research and development, the target-based drug discovery strategy is often used [10]. This method identifies the disease-specific targets and target-specific drugs to achieve precise therapy. Similarly, we believe that the application of a target-ingredient-herb interaction network may also help to discover new effective TCM prescriptions for complex diseases with multi-targets.

In this study, we developed a multiple target-oriented gradient weighting strategy to tailor TCM prescriptions for complex diseases. This strategy merges ancient TCM theories with modern scientific insights, particularly in pharmacology and disease pathophysiology. By incorporating a systematic data-driven approach (target-herbal ingredient-TCM herb interaction) and weighting interactions between disease targets and herbal components, the method helps to optimize the prescription by covering multiple biological pathways, thus improving treatment outcomes. Moreover, this new strategy introduces a more quantitative evidence-based methodology that uses a gradient weighting system to fine-tune the selection of herbs and their dosages. Consequently, the precision of TCM formulations can be improved, making them more reliable and reproducible in clinical practice. This strategy enables the identification of novel combinations of herbs or herbal components and creates more standardized prescriptions, potentially accelerating the integration of TCM into modern healthcare systems and contributing to the growing field of personalized medicine.

Intracerebral hemorrhage (ICH) is a fatal disease. Its pathophysiology involves primary assault (mass effect) and secondary injuries (brain edema, neuroinflammation, and oxidative stress, etc.) [11]. Currently, no specific treatment is available for ICH [11]. In addition, most mono-target drugs failed to improve the neurological outcomes of patients with ICH in clinical trials [11,12]. Thus, polypharmacy may be an alternative strategy for improving ICH outcomes [12,13]. In the TCM theory, the pathological features of ICH are the interaction of blood stasis, phlegm, and heat, etc.. Promising therapeutic effects of several TCM prescriptions have been reported on ICH, such as Buyang Huanwu decoction, Xuefu Zhuyu decoction (XFZYD), and Liangxue Tongyu decoction [7,9,14,15]. However, a pathophysiologically customized TCM prescription for ICH is still lacking.

Therefore, we selected ICH as an example and formulated a tailored prescription based on our new strategy. Expert evaluations and animal experiments validated the rationality and efficacy of the novel TCM formula (Fig. 1).

2. Material and methods

2.1. Screening of ICH targets

The ICH-related genes were screened by searching“intracerebral hemorrhage” in the GeneCards database (https://www.genecards.org/) [16]. The top 100 genes and the relevance score were used for further analyses.

2.2. Screening of the target-related ingredients and ingredient-containing herbs

The target-related ingredients were searched using the SymMap database (http://www.symmap.org; version: 2.0) by inputting the top 100 ICH-related genes [17]. Ingredients with an oral bioavailability (OB) > 30% were included. Then, the resulting ingredients were entered into Traditional Chinese Medicine Systems Pharmacology (TCMSP) (https://tcmsp-e.com/tcmsp.php; version: 2.3) to gain the ingredient-containing herbs [18]. The disease-target-ingredients-herb network was constructed by Cytoscape (version 3.9.1).

2.3. Formulation of the new TCM prescription

The relevance of ingredients and herbs to ICH was determined using the cumulative relevance scores of the corresponding targets, as shown in Eqs. (1) and (2) below:

$$\text{Score } B = \sum_{i=1}^{n} \text{Score } Ai \tag{1}$$

$$\text{Score } C = \sum_{i=1}^{m} \text{Score } Bi \tag{2}$$

Score *A* refers to the relevance of the target to ICH, score *B* refers to the relevance of the ingredient to ICH, and score *C* refers to the relevance of the herb to ICH. *i* is the summation variable for the arithmetic formula $\sum$. It ranges from the starting value to the ending value. *n* refers to the number of targets related to a specific ingredient. *m* refers to the number of ingredients in a herb.

Based on the ranking of the integrated relevance scores, a new TCM prescription that consists of the top-scoring herbs was formulated when the cumulative score, number of ingredients, and number of targets of the herbs did not increase with the number of herbs. In this prescription, the composition and ratios of the herbs were determined by the rank and ratios of the scores, respectively.

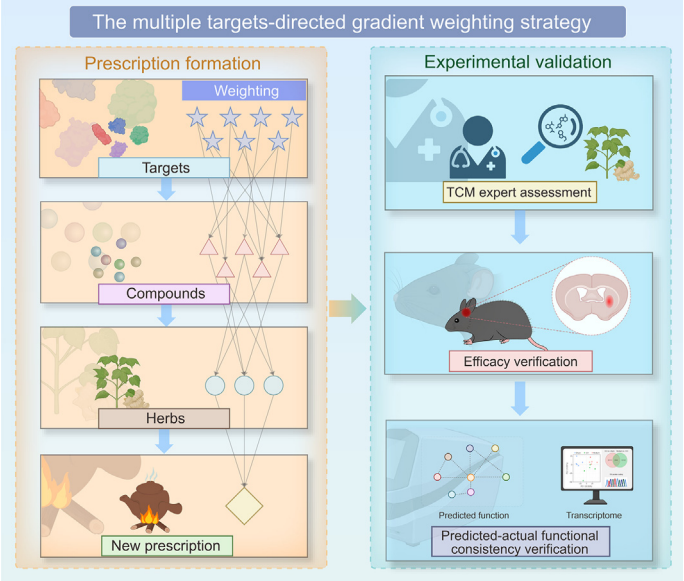

Fig. 1. Flow chart of this study. The targets of diseases, target-binding ingredients, and ingredient-containing herbs were collected. The relevance scores are gradient weighted. A new traditional Chinese medicine (TCM) prescription is formulated according to the rank of the relevant score. The rationality and effectiveness of the new prescriptions are validated in a mouse model of intracerebral hemorrhage (ICH). PC: principal component.

2.4. Expert verification

Experienced Chinese physicians, Prof. Tao Tang (Institute of Integrative Medicine, Department of Integrated Traditional Chinese and Western Medicine, Xiangya Hospital, Central South University, Jiangxi (National Regional Center for Neurological Diseases), China) and Prof. Jiekun Luo (Institute of Integrative Medicine, Department of Integrated Traditional Chinese and Western Medicine, Xiangya Hospital, Central South University, China), confirmed the rationality of the new TCM prescription.

2.5. Animals

Male C57 BL/6J mice (12 weeks old) were purchased from Hunan Slake Jingda Laboratory Animal Co., Ltd. (Changsha, China). The animals were housed in accordance with the Animals (Scientific Procedures) Act 1986. All protocols were approved by the Center of Laboratory Animals at Xiangya Hospital Central South University, China (Approval No.: XY-20240312003).

2.6. Animal models

The mice were anesthetized using 0.3% pentobarbital sodium (60 mg/kg) and fixed on a stereotaxic instrument. ICH was induced by injecting type VII collagenase (0.075 U/0.5 μL, C0773; Sigma, St. Louis, MO, USA) into the right globus pallidum (0.5 mm behind, 2.0 mm right to the bregma, and 4.0 mm below the skull). An equal volume of distilled normal saline was used to replace collagenase in the sham animals. The mice were kept on a thermostatic heating pad to maintain their body temperature until they awoke. Additional soft food and accessible water were available to the postoperative mice.

2.7. Doses and preparation of TCM formula

Dried herbs were obtained from the TCM Pharmacy of Xiangya Hospital, Central South University (Changsha, China). The prescriptions (Nao Yi Kang decoction (NYKD)) consisted of *Hippophae rhamnoides* L. (Hippophae Fructus), *Ginkgo biloba* L. (Ginkgo Folium), *Achyranthes bidentata* Blume (Achyranthis Bidentatae Radix), *Scutellaria barbata* D. Don (Scutellariae Barbatae Herba), and *Carthamus tinctorius* L. (Carthami Flos) at a ratio of 1:1:1:1:1 (*m/m*, Table 1 [19]) according to their weighted scores. Plant names were checked from http://www.theplantlist.org. According to the Chinese Pharmacopoeia (2020 edition) [19], 9 g of each herb are used by adult men weighing 70 kg. The human dose was then converted to a medium dose for mice (5.79 g/kg) based on body surface area. The low and high doses were half and two times the medium dose, respectively. As positive control, XFZYD is composed of 11 herbs (Table S1), and the dose of XFZYD was 12 g/kg (raw herbs) [20].

The mixed herbs were soaked twice (1 h in distilled water), followed by decoction for 30 min. The extracts were then mixed, filtered, and evaporated to obtain high concentrations. The resulting solution was stored at −80 °C. The high-dose decoction was diluted to medium and low doses with distilled water immediately prior to use.

2.8. Experimental design and drug administration

Part 1: the mice were randomly assigned to five groups: sham, ICH, low-dose (Low), medium-dose (Medium), and high-dose (High). Part 2: the mice were randomly assigned to one of three groups: ICH, XFZYD, or NYKD. All mice underwent ICH or sham surgery. The Longa test was performed after awaking up from anesthesia. Mice with a Longa score of zero in the post-ICH groups were excluded. Then, 0.4 mL of distilled water or TCM extracts were daily administrated by gavage for three days. On days 1 and 3 after ICH, the modified neurological severity score (mNSS) and foot fault rate were recorded. The serum and brains were collected on the third day after modeling.

2.9. Neurobehavioral test

2.9.1. mNSS

The mNSS was evaluated as previously reported [8,13]. It includes motor, sensory, reflex, and balance tests. The mNSS grades range from 0 to 18. A higher score indicates worse performance.

2.9.2. Foot fault test

The mice were placed on a 2.5 cm × 2.5 cm grid. The number of total and slipped steps in the forepaws within 1 min was recorded. Foot fault rates were calculated as (contralateral faults-ipsilateral faults)/total steps [8,13].

2.10. Blood coagulation assays

Prothrombin time (PT), activated partial thromboplastin time (APTT), and fibrinogen (FIB) content were examined according to the manufacturer's recommendations (R01002, R01102, and R01302; Rayto Life and Analytical Sciences Co., Ltd., Shenzhen, China) by a fully automatic blood coagulation analyzer (RAC-1830; Rayto Life and Analytical Sciences Co., Ltd.).

2.11. Quality control of the TCM formula

The blood of mice was collected at 1 h after drug administration through the angular vein under anesthesia. Serum was then isolated.

The herbal ingredients of the herb in extracts and serum were detected using an ultra-performance liquid chromatography (UPLC) (Vanquish; Thermo Fisher Scientific Inc., Waltham, MA, USA)-tandem mass spectrometry (MS/MS) (Q Exactive Focus; Thermo Fisher Scientific Inc.) system. Qualitative analyses of the primary and secondary MS data were performed by referencing a

Table 1
Composition of Nao Yi Kang decoction (NYKD) [19].

Chinese name	Latin name	Relevant scores[a]	Recommended doses (g) [19]	Part used	Origin area	Batch number	Ratios used (*m*/*m*)[b]
Sha Ji	*Hippophae rhamnoides* L.	2420.33	3–10	Fruit	Xinjiang, China	710220901	9
Yin Xing Ye	*Ginkgo biloba* L.	2241.68	9–12	Leaf	Hunan, China	19052909	9
Niu Xi	*Achyranthes bidentata* Blume	2082.87	5–12	Root	Henan, China	23122910	9
Ban Zhi Lian	*Scutellaria barbata* D. Don	2071.42	9–15	Whole plant	Sichuan, China	C061210701	9
Hong Hua	*Carthamus tinctorius* L.	2008.89	3–10	Flower	Xinjiang, China	23081106	9

[a] The cumulative relevant scores of each herb to intracerebral hemorrhage.
[b] The ratios we used in animal experiments.

self-built MS database based on reference standards. Mixed quality control samples and internal standards (L-2-chlorophenylalanine) were used to examine the stability of the UPLC-MS/MS system.

2.12. Histopathological, immunohistochemical, and immunofluorescence examination

The paraffin-embedded sections were used for staining. Slices were deparaffinized and rehydrated prior to staining. For hematoxylin and eosin (H&E) staining, the slices were stained with hematoxylin (G1004; Servicebio, Wuhan, China) and eosin Y (G1001; Servicebio) for 5 min and 20 s, respectively. The Nissl bodies of the neurons were visualized after 8 min of staining in toluidine blue (G1036; Servicebio). Apoptotic cells were detected using the terminal deoxynucleotidyl transferase-mediated deoxyuridine triphosphate nick-end labeling (TUNEL) kit (MA0224; Meilunbio, Dalian, China). Immunoglobin leakage into the brain was assessed by immunohistochemistry using an anti-mouse immunoglobulin G (IgG)-horseradish peroxidase (HRP) polysome kit (SV0001; Boster Biological Technology Co., Ltd., Wuhan, China).

For immunofluorescence, the slices were boiled in citrate buffer (pH 6.0, 100 °C, 20 min), incubated with primary antibodies (4 °C, 18 h), secondary antibodies (room temperature, 1 h), and 4′,6-diamidino-2-phenylindole (DAPI) (C0065; Solarbio, Beijing, China, room temperature, 5 min), subsequently. The primary antibodies used were mouse anti-glial fibrillary acidic protein (GFAP) (1:1500, CSB-MA009369A0m; Cusabio Biotech Co., Ltd., Wuhan, China), mouse anti-proliferating cell nuclear antigen (PCNA) (1:1000, 2586; Cell Signaling Technology, Danvers, MA, USA), rabbit anti-ionized calcium-binding adaptor molecule 1 (Iba1) (1:500, 17198; Cell Signaling Technology), rabbit anti-PCNA (1:1000, 13110; Cell Signaling Technology), rabbit anti-cluster of differentiation 86 (CD86) (1:200, 19589; Cell Signaling Technology), and rabbit anti-arginase 1 (Arg1) (1:1000, 93668; Cell Signaling Technology). Secondary antibodies were Alex flour 488-conjugated donkey anti-mouse IgG (H+L) (1:1000, 715-545-150; Jackson ImmunoResearch, West Grove, PA, USA), Alex flour 488-conjugated donkey anti-rabbit IgG (H+L) (1:1000, 711-545-152; Jackson ImmunoResearch), Cy3-conjugated donkey anti-mouse IgG (H+L) (1:1000, 715-165-150; Jackson ImmunoResearch), and Cy3-conjugated donkey anti-rabbit IgG (H+L) (1:1000, 711-165-152; Jackson ImmunoResearch). For double staining of Iba1/CD86 and Iba1/Arg1, a tyramide signal amplification system was used according to the manufacturer's instructions (AFIHC023; Hunan Aifang Biotechnology Co., Ltd., Changsha, China).

The stained slices were scanned using a Pannoramic Midi Scanner (3DHISTECH Kft, Budapest, Hungary) and processed with the Caseviewer 2.3 (3DHISTECH Kft). Fluorescent images were obtained using an M2 Imager microscope (Carl Zeiss AG, Oberkochen, Germany).

2.13. Transcriptomic analysis

Total RNA was extracted from the right globus pallidus tissue. Complementary DNA (cDNA) libraries were prepared using a TruSeq Stranded Total RNA Library Prep Kit (RS-122-2001, Illumina, Inc., San Diego, CA, USA), amplified by polymerase chain reaction (PCR), and purified using AMPure XP beads (Beckman Coulter, Brea, CA, USA). Sequencing was performed by Novogene Co., Ltd. (Beijing, China) on a NovaSeq™ X Plus system (Illumina, Inc.).

Sequencing data were analyzed using the NovoMagic platform. The differentially expressed genes (DEGs) were screened using the edgeR package (3.22.5) that integrated $P < 0.05$ and fold change (FC) > 2 or FC < 0.5. Enrichment, protein-protein interaction (PPI), gene localization, and transcription factor analyses were performed using Metascape (https://metascape.org/). The parameters used for Metascape analyses were set to default.

2.14. Statistical analysis

All data were analyzed by investigators who were blinded to the grouping information. High-throughput data were analyzed using Student's *t*-test. Other data were analyzed using one-way analysis of variance (ANOVA) and Dunnett's test with the aid of GraphPad 10.0. $P < 0.05$ was considered to be statistically significant. Data are presented as mean ± standard deviation (SD).

3. Results

3.1. The targets of ICH

We screened ICH-related targets on the GeneCards databases based on relevance scores. The top 100 genes included *COL4A1*, *ACE*, and *COL4A2*. (Table S2). PPI analysis showed that the core targets were related to inflammation (*IL6*, *IL1B*, *TNF*, *CXC3L*, etc.), coagulation cascade (*PLAT*, *F2*, *F3*, *vWF*, etc.), and vascular remodeling (*MMP9*, *TGFB1*, etc.) (Fig. S1A). Gene Ontology (GO) analysis indicated that the top 100 genes were associated to glia cell (astrocyte) activation and development, vascular damage and remodeling, blood coagulation, and inflammatory processes (Fig. S1B).

3.2. The ICH-targeting herbal ingredients

Potential ICH-curative herbal ingredients were collected from the SymMap database and filtered using OB. The top 100 targets were linked to 1904 ingredients. The predicted OB of the 488 ingredients was greater than 30% (Table S3). As weighted by the cumulative relevance score to ICH, (−)-epigallocatechin-3-gallate, quercetin, and wogonin were the top three components for ICH (the largest rectangle, Fig. 2A).

3.3. The potential ICH-curative herbs

The ingredients-containing herbs were searched in the TCMSP database. Their curative effects were quantified by the cumulative relevance score of ingredient-ICH interactions. The results indicated that *Hippophae rhamnoides* L. (Hippophae Fructus), *Ginkgo biloba* L. (Ginkgo Folium), *Achyranthes bidentata* Blume (Achyranthis Bidentatae Radix), *Scutellaria barbata* D. Don (Scutellariae Barbatae Herba), and *Carthamus tinctorius* L. (Carthami Flos) were the top five potential drugs for ICH treatment (Fig. 2B and Table S4). In addition, the top ingredients only partially contributed to the cumulative scores (Fig. S2A) and proportions (Fig. S2B) for each herb, suggesting the multi-component and multi-functional properties of the herbs.

3.4. The ICH-tailored TCM formula and the related targets

Based on the trends of the number of ingredients, the number of targets, and the cumulative relevance socres (Figs. 2C–E), the top five herbs were selected to form a new TCM prescription. The herbs used were Hippophae Fructus, Ginkgo Folium, Achyranthis Bidentatae Radix, Scutellariae Barbatae Herba, and Carthami Flos. According to the relevance score ratios, the constituent ratios of the five herbs were 1:1:1:1:1 (*m*/*m*). The experienced Chinese

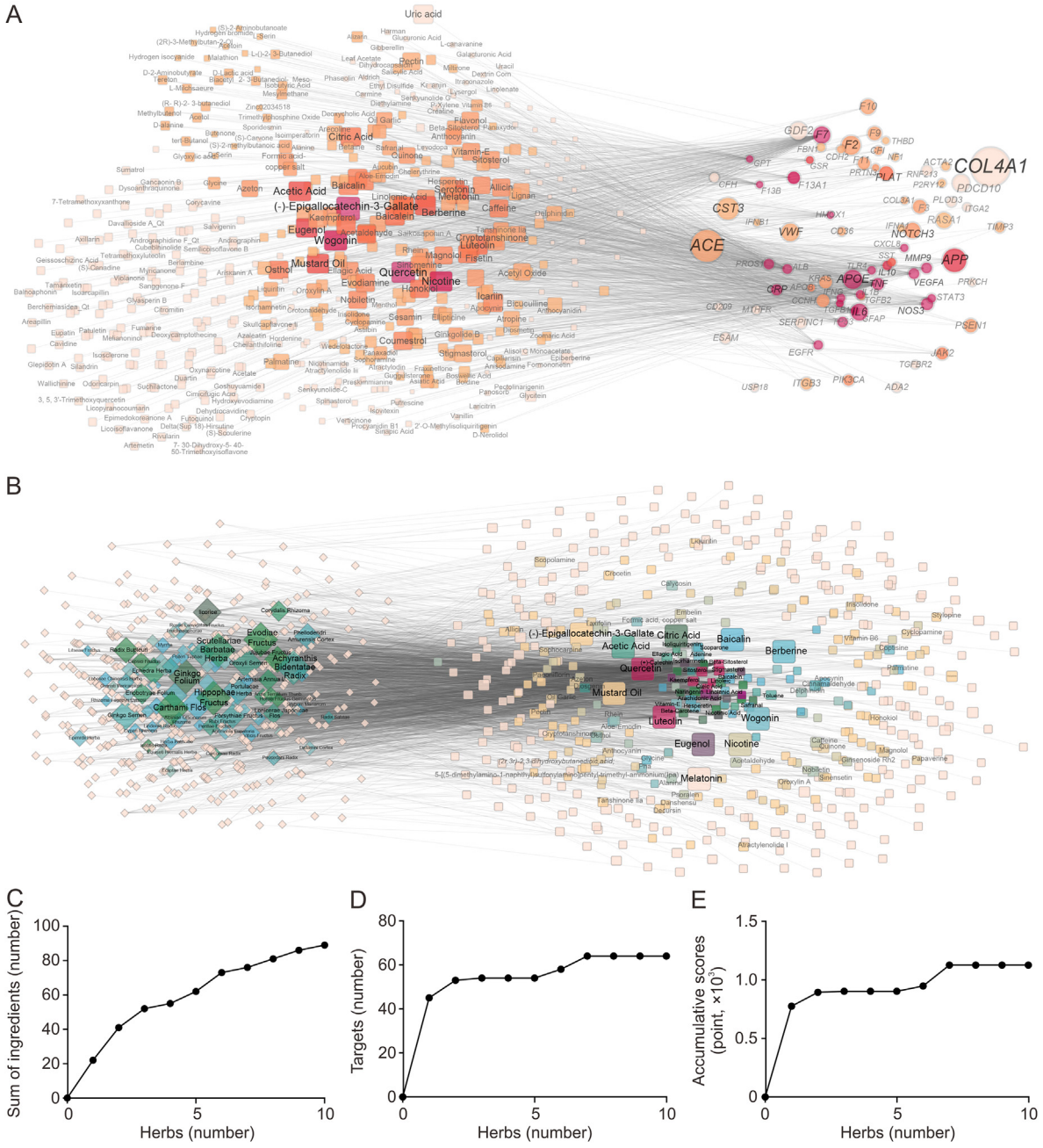

Fig. 2. The target-ingredient and ingredient-herb networks for intracerebral hemorrhage (ICH). (A) The network of ICH-related targets (circle) and herbal ingredients (square). (B) The network of the target-related ingredients (square) and ingredient-containing herbs (diamond). For each symbol, the size represents the relevant scores. The color represents the number of links, the redder, the more. (C–E) The number of ingredients (C), the number of targets (D), and the cumulative relevance scores (E) increase slowly when the number of herbs is larger than 5.

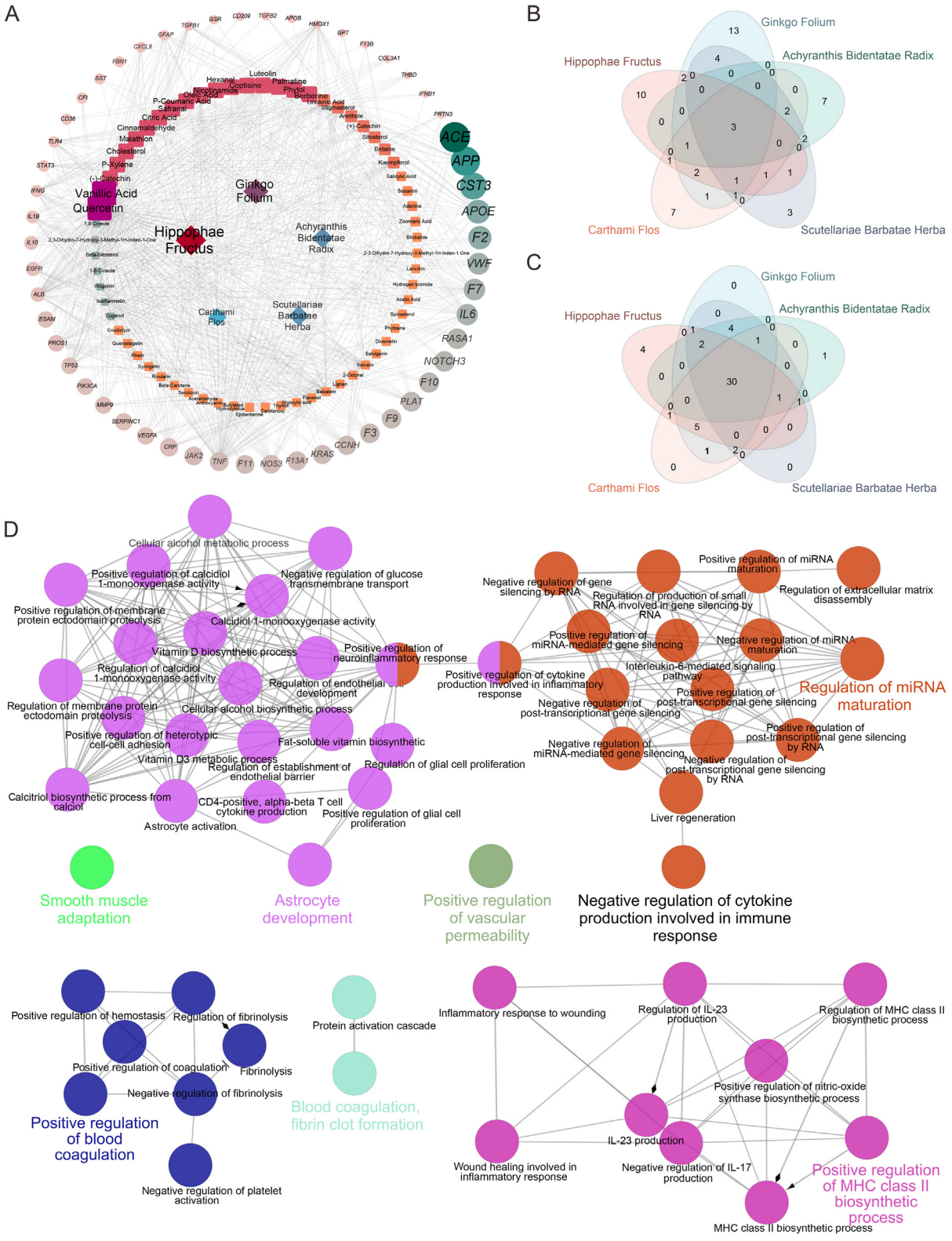

Fig. 3. The intracerebral hemorrhage (ICH)-tailored traditional Chinese medicine (TCM) prescription. (A) The target (circle)-ingredient-(square)-herb network of the top five scored herbs. (B) Venn diagram of the top five herbs-contained ingredients. (C) Venn diagram of the top five herbs-related ICH targets. (D) Gene Ontology (GO) analysis predicts that Nao Yi Kang decoction (NYKD) may regulate glial cell development, blood coagulation, vascular permeability, and neuroinflammation. CD4: cluster of differentiation 4; miRNA: microRNA; IL: interleukin; MHC: major histocompatibility complex.

physicians confirmed the rationality of the composition from the perspective of TCM theory: the function of the formula is "promoting the blood circulation to remove stasis and clearing heat for detoxification". Specifically, the monarchs are Ginkgo Folium (promoting the blood circulation and removing stasis) and Scutellaria Barbatae Herba (clearing heat and detoxification), the ministers are Carthami Flos (promoting the blood circulation) and Achyranthis Bidentatae Radix (clearing heat), the assistant is Hippophae Fructus (promoting blood circulation, protecting the spleen and stomach, and preventing gastrointestinal complications), and the guide is Achyranthis Bidentatae Radix (guiding the stasis and heat toxins downward). Because the formula was tailored for ICH (named Nao Yi Xue in Chinese), we named it NYKD (Table 1).

Then, we constructed an ICH-target-ingredient-herb network of NYKD, based on the ICH-target, target-ingredient, and ingredient-herb interactions (Fig. 3A). The network contained 5 herbs, 62 ingredients, and 54 targets (Fig. 3A). This complex network reflects the multiple roles of NYKD in post-ICH pathophysiology. In this network, 3 ingredients (quercetin, beta-sitosterol, and stigmasterol) and 30 targets were shared among the five herbs (Figs. 3B and C).

GO analysis of NYKD-related ICH targets also revealed the multifunctionality of the prescription, including the regulation of glial cell development and activation, vascular permeability, neuroinflammation, and blood coagulation (Fig. 3D).

3.5. The absorption of the potential ICH-curative ingredients

UPLC-MS/MS suggested that among all the ingredients detected in NYKD solution and serum from NYKD treated mice, 22 ingredients were predicted to be ICH-curative by our strategy, including quercetin, wogonin, baicalin, bilobalide, and kaempferol (Fig. 4 and Tables 2 and S5).

3.6. The therapeutic effects of the ICH-tailored TCM prescription

In the mouse model of ICH, NYKD improved the mNSS and foot fault rate on the third day after ICH (Figs. 5A and B). Particularly, the medium dose exhibited a remarkable curative effect. In addition, the medium dose of NYKD substantially reduced the hematoma volume (Figs. 5C and D). Furthermore, H&E staining showed improved perihematomal cell disorganization, extracellular matrix degradation, and neuroinflammation in the NYKD groups compared to those in the ICH group (Fig. 5E). Nissl staining also indicated that the number of survival neurons increased after NYKD treatment (Figs. 5F and G). Moreover, brain IgG leakage (Figs. 5H and I) and apoptosis (Figs. 5J and K) was mitigated by NYKD. Taken together, NYKD was effective in a mouse model of ICH, with the medium dose showing more remarkable effects. Therefore, we selected the medium dose for further investigations. Additional experiments indicated that the efficacy of NYKD was equivalent to that of the classical TCM prescription XFZYD as assessed by mNSS (Fig. S3A), foot fault rate (Fig. S3B), H&E (Fig. S3C), Nissl (Figs. S3D and E), IgG leakage (Figs. S3F and G), and TUNEL staining (Figs. S3H and I).

3.7. No general side effects were detected for the ICH-tailored TCM prescription

To evaluate the side effects of NYKD on other tissues, histological examination of the heart, liver, spleen, lung, and kidney slides using H&E demonstrated no obvious structural changes among the groups (Fig. S4A). Moreover, NYKD may regulate blood coagulation, which is thought to affect hematoma expansion in the acute stage. However, our blood coagulation tests showed no significant differences between the ICH and NYKD groups in terms of the extrinsic coagulation pathway (PT),

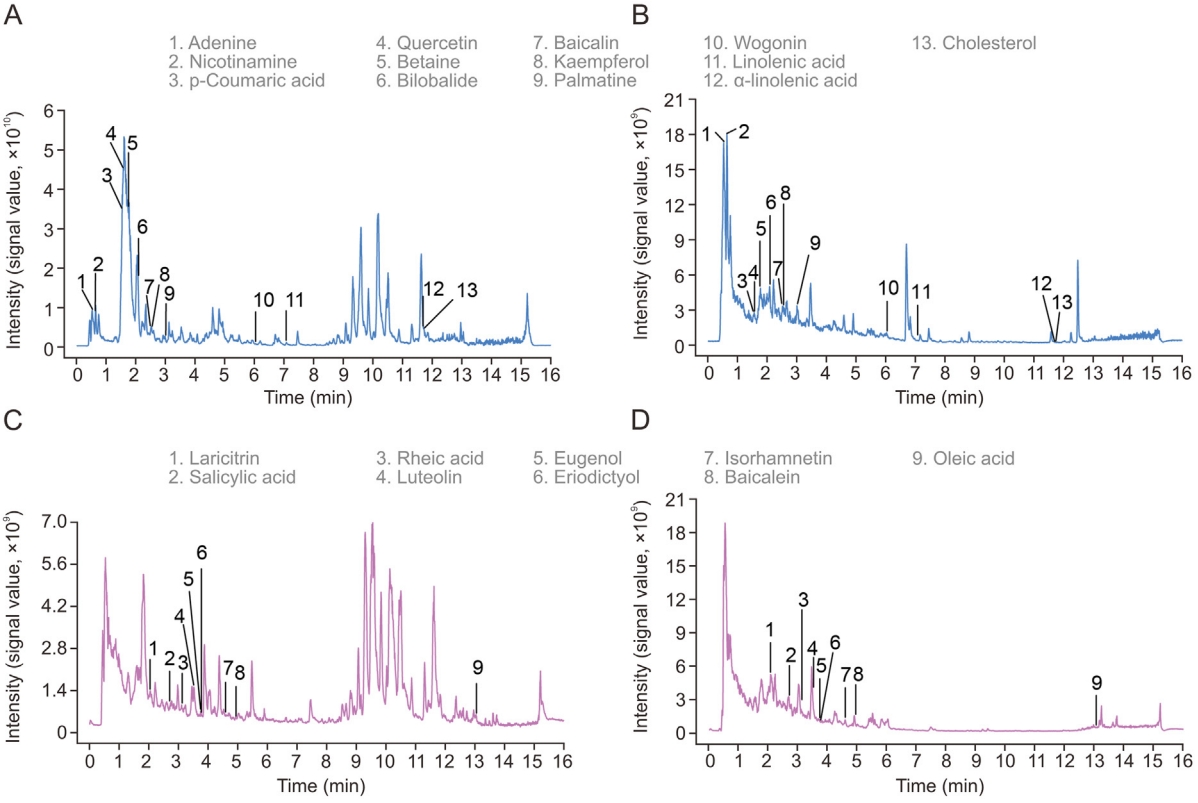

Fig. 4. The active ingredients in Nao Yi Kang decoction (NYKD) solution and mice serum. (A, B) The active ingredients in mice serum (A) and in NYKD solution (B) at positive mode. (C, D) The active ingredients in mice serum (C) and in NYKD solution (D) at negative mode.

Table 2
The detected intracerebral hemorrhage (ICH) curative active ingredients in Nao Yi Kang decoction (NYKD) and mice serum.

Name	MS^2 score	Formula	*m/z*	Retention time (s)	MS adduct	*m/z* of MS^2 fragments	Related herbs
Adenine	1.00	$C_5H_5N_5$	136.0552	32.2897	$[M+H]^+$	136.062167, 119.035705, 137.045898, 131.019544, and 91.053894	*Carthamus tinctorius* L.
Nicotinamine	1.00	$C_6H_6N_2O$	123.0553	37.7325	$[M+H]^+$	123.055377, 124.038807, 80.049138, 95.048961, and 96.044514	*Hippophae rhamnoides* L.
p-Coumaric acid	0.94	$C_9H_8O_3$	165.0549	91.3795	$[M+H]^+$	147.04454, 119.049286, 91.054023, 165.091921, and 123.043796	*Scutellaria barbata* D. Don *Ginkgo biloba* L.
Quercetin	0.99	$C_{15}H_{10}O_7$	303.0500	93.9897	$[M+H]^+$	303.049448, 229.049883, 285.039962, 257.044977, and 153.017905	*Scutellaria barbata* D. Don *Carthamus tinctorius* L., *Achyranthes bidentata* Blume, *Hippophae rhamnoides* L., and *Ginkgo biloba* L.
Betaine	0.98	$C_5H_{11}NO_2$	118.0862	105.0160	$[M+H]^+$	118.086677, 59.073245, 58.065298, 92.656944, and 72.080654	*Achyranthes bidentata* Blume
Bilobalide	0.96	$C_{15}H_{18}O_8$	327.1077	125.5150	$[M+H]^+$	309.097004, 327.108832, 57.070268, 111.080769, and 149.060873	*Ginkgo biloba* L.
Baicalin	0.94	$C_{21}H_{18}O_{11}$	447.0916	149.1695	$[M+H]^+$	271.058168, 447.090459, 153.017924, 272.063973, and 68.997327	*Scutellaria barbata* D. Don, *Carthamus tinctorius* L., and *Achyranthes bidentata* Blume
Kaempferol	0.99	$C_{15}H_{10}O_6$	287.0554	152.9930	$[M+H]^+$	287.055001, 153.018358, 121.029395, 92.658643, and 165.017607	*Carthamus tinctorius* L., *Achyranthes bidentata* Blume, *Hippophae rhamnoides* L., and *Ginkgo biloba* L.
Palmatine	0.74	$C_{21}H_{22}NO_4^+$	352.1525	181.0270	$[M]^+$	352.15218, 180.137281, 334.140132, 198.148986, and 278.113424	*Achyranthes bidentata* Blume
Wogonin	0.97	$C_{16}H_{12}O_5$	285.0757	362.4535	$[M+H]^+$	285.077476, 270.053843, 57.069865, 284.293968, and 92.658769	*Scutellaria barbata* D. Don and *Achyranthes bidentata* Blume
Linolenic acid	0.81	$C_{18}H_{30}O_2$	279.2321	424.1690	$[M+H]^+$	149.023728, 121.100729, 175.148048, 81.069544, and 95.085847	*Carthamus tinctorius* L., *Hippophae rhamnoides* L., and *Ginkgo biloba* L.
Alpha-linolenic acid	0.98	$C_{18}H_{30}O_2$	279.2321	701.3240	$[M+H]^+$	81.069644, 67.054343, 95.085062, 279.233949, and 109.101022	*Carthamus tinctorius* L., *Hippophae rhamnoides* L., and *Ginkgo biloba* L.
Cholesterol	0.98	$C_{27}H_{46}O$	369.3518	703.9790	$[M+H]^+$	369.354642, 147.117442, 161.132647, 109.101031, and 95.085643	*Scutellaria barbata* D. Don, *Carthamus tinctorius* L., and *Hippophae rhamnoides* L.
Laricitrin	0.92	$C_{16}H_{12}O_8$	331.0455	122.3410	$[M-H]^-$	303.047885, 275.057593, 331.045518, 92.675964, and 151.003699	*Ginkgo biloba* L.
Salicylic acid	0.98	$C_7H_6O_3$	137.0244	161.9880	$[M-H]^-$	93.034843, 136.892189, 108.900204, 138.018549, and 94.037699	*Carthamus tinctorius* L.
Rheic acid	0.81	$C_{15}H_8O_6$	283.0248	187.4605	$[M-H]^-$	283.026162, 255.028606, 117.035045, 163.004024, and 72.992894	*Hippophae rhamnoides* L.
Luteolin	0.99	$C_{15}H_{10}O_6$	285.0404	210.8780	$[M-H]^-$	285.041868, 133.028612, 151.003994, 286.044102, and 175.039365	*Scutellaria barbata* D. Don, *Carthamus tinctorius* L., and *Ginkgo biloba* L.
Eugenol	0.92	$C_{10}H_{12}O_2$	163.0764	224.7510	$[M-H]^-$	148.053004, 162.838303, 119.050163, 149.057401, and 73.070954	*Ginkgo biloba* L.
Eriodictyol	0.78	$C_{15}H_{12}O_6$	287.0561	225.3950	$[M-H]^-$	151.004012, 135.044843, 92.67609, 287.05604, and 107.013419	*Scutellaria barbata* D. Don
Isorhamnetin	0.99	$C_{16}H_{12}O_7$	315.0506	275.2680	$[M-H]^-$	315.051016, 300.029736, 151.004252, 271.022891, and 164.011172	*Hippophae rhamnoides* L. and *Ginkgo biloba* L.
Baicalein	0.99	$C_{15}H_{10}O_5$	269.0457	296.4805	$[M-H]^-$	269.044942, 92.68033, 268.164064, 79.957557, and 149.571221	*Scutellaria barbata* D. Don, *Carthamus tinctorius* L., and *Achyranthes bidentata* Blume
Oleic acid	0.95	$C_{18}H_{34}O_2$	281.2482	783.1875	$[M-H]^-$	281.246419, 82.308617, 206.352121, 246.280228, and 135.280018	*Scutellaria barbata* D. Don, *Carthamus tinctorius* L., *Hippophae rhamnoides* L., and *Ginkgo biloba* L.

MS: mass spectrometry.

intrinsic coagulation pathway (APTT), or FIB. Although APTT tended to increase, FIB tended to decrease after NYKD treatment (Figs. S4B–D).

3.8. The effects of the ICH-tailored TCM prescription on brain transcriptomics

To further reveal the multi-target effects of NYKD on ICH, we performed brain transcriptomics after ICH and NYKD treatment. The principal component analysis (PCA) plot suggested distinct transcriptomic profiles between the ICH and NYKD groups (Fig. 6A). Most of the DEGs (1925/2405) were upregulated in the ICH group compared to those in the sham group (Fig. 6B), whereas most of the DEGs (1495/1806) were downregulated in the NYKD group compared to those in the ICH group (Fig. 6C). Among the differential genes, 294 overlapped between the ICH vs. sham and NYKD vs. ICH comparisons, and 150 were identified as protein-coding genes (Fig. 6D). Functional analysis indicated that the NYKD-regulated genes were mostly enriched in the processes of cell activation and development (regulation of cell activation, leukocyte activation, and response to growth factor), vascular permeability and remodeling (extra cellular matrix (ECM) proteoglycans, extracellular matrix assembly, elastic fiber formation, and basement membrane organization), and inflammation (inflammation responses, leukocyte activation, and chemokine production) (Fig. 6E and Table S6), which were well-matched with the results of GO analysis of the NYKD-related ICH targets (Fig. 3D), although only one DEG overlapped with the potential targets (Fig. S5).

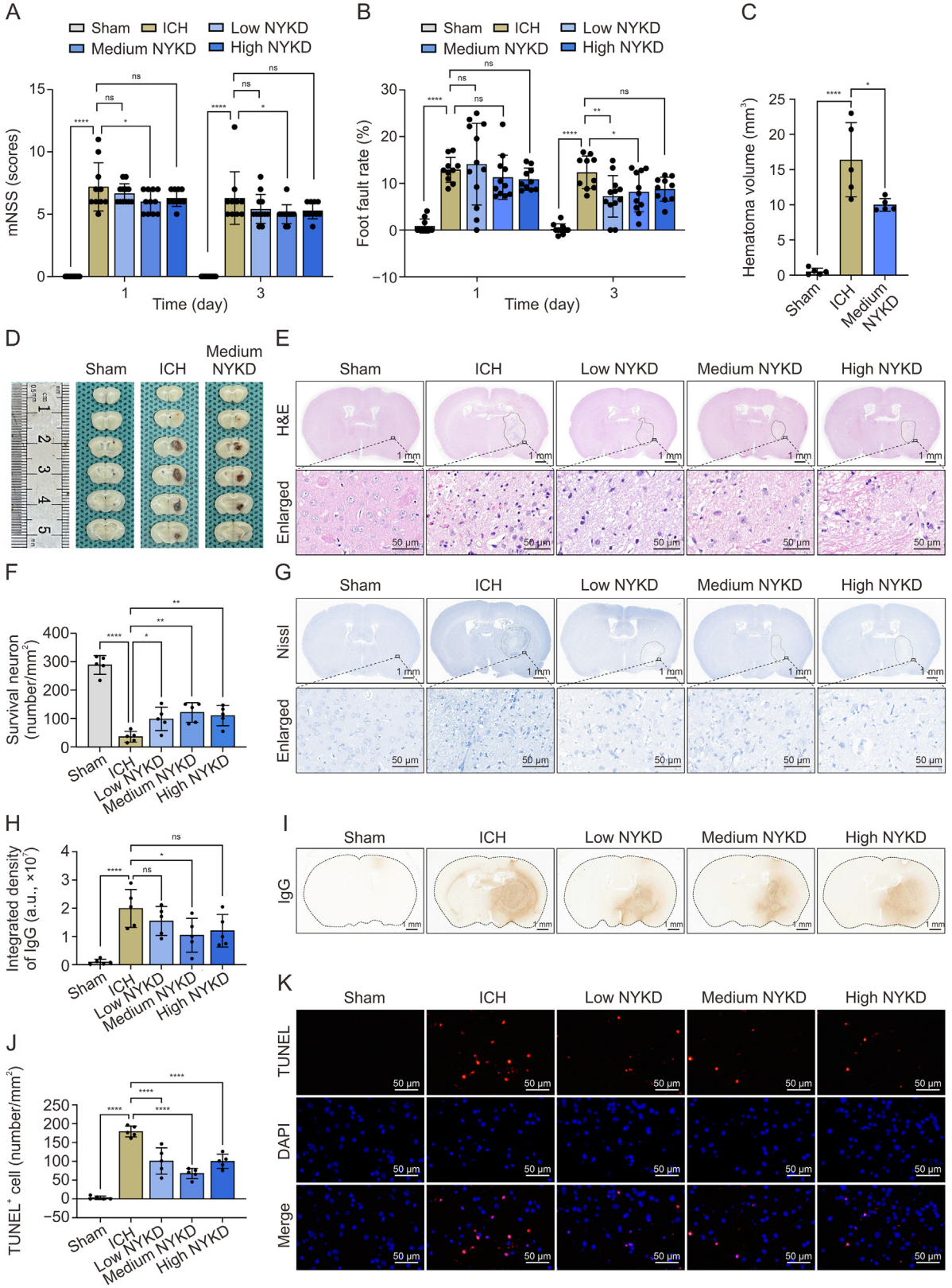

Fig. 5. The effects of Nao Yi Kang decoction (NYKD) on intracerebral hemorrhage (ICH). (A) The medium dose of NYKD substantially improved the modified neurological severity score (mNSS) of ICH mice in the acute stage. (B) The medium dose of NYKD significantly reduces the foot fault rate after ICH. (C, D) The medium dose of NYKD substantially reduced the hematoma volume after ICH: statistic diagram of hematoma volume (C) and representative diagram of brain slices showing hematoma volume (D). (E) Hematoxylin and eosin (H&E) staining suggests that NYKD reversed the pathohistological abnormalities after ICH. (F, G) Nissl staining indicates that NYKD increased the number of survival neurons around the hematoma: statistic diagram of survival neurons (F) and representative images of Nissl staing (G). (H, I) Immunohistochemical analysis of immunoglobulin G (IgG) shows that NYKD ameliorated vascular leakage: statistic diagram of the integrated density of IgG (H) and representative images of IgG staining (I). (J, K) Terminal deoxynucleotidyl transferase-mediated deoxyuridine triphosphate nick-end labeling (TUNEL) displays that NYKD suppressed the post-ICH cell apoptosis: statistic diagram of the number of TUNEL positive cells (J) and representative images of TUNEL staining (K). Data are presented as mean ± standard deviation (SD) ($n = 10–12$ in Figs. 5A and B; $n = 5$ in Figs. 5C–K). $^{*}P < 0.05$, $^{**}P < 0.01$, and $^{****}P < 0.0001$. ns: not significant. Low: low dose; Medium: medium dose; High: high dose;DAPI: diamidino-phenyl-indole.

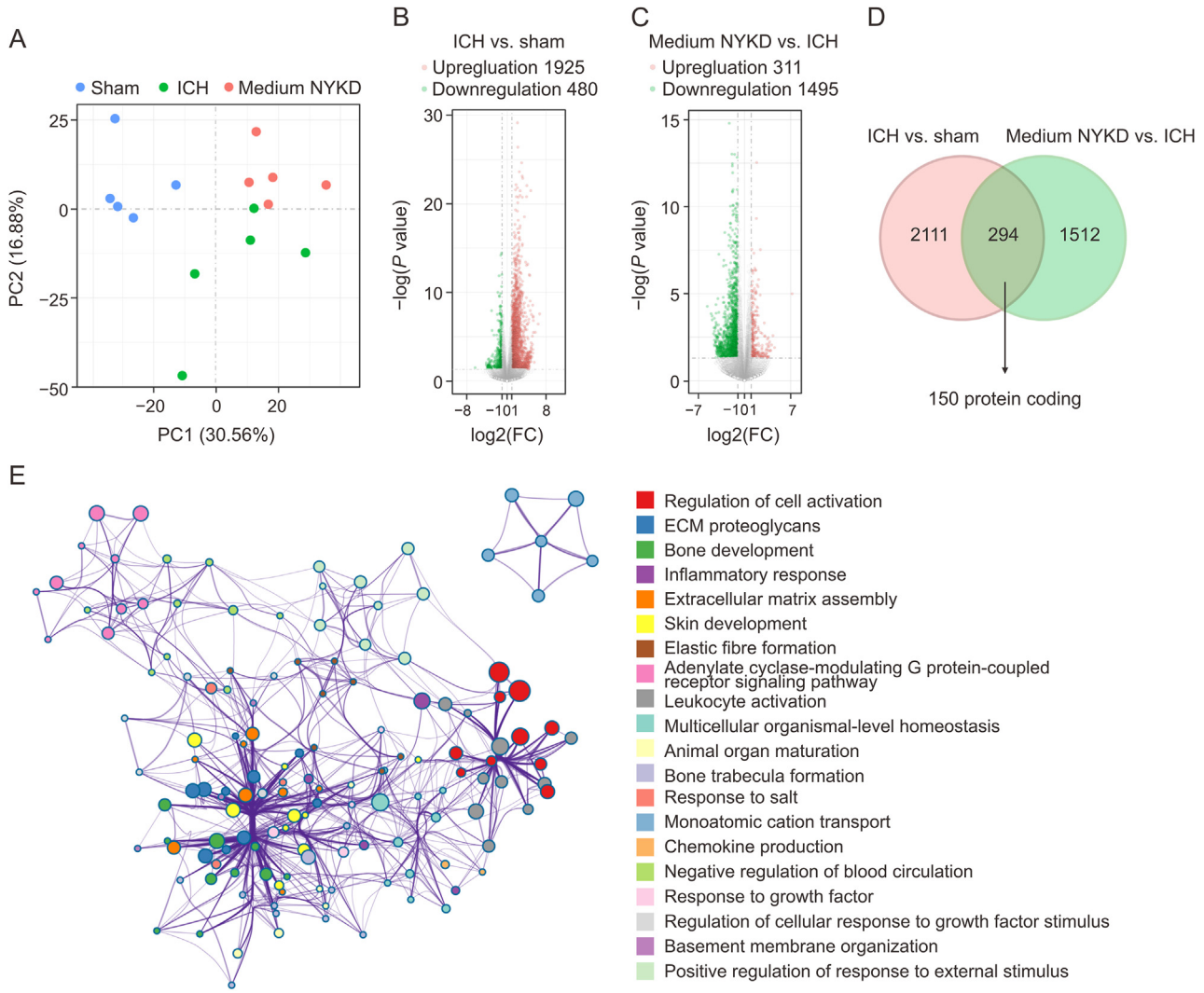

Fig. 6. The effects of Nao Yi Kang decoction (NYKD) on the brain transcriptional profiles. (A) Principal component analysis (PCA) plot shows distinct transcriptional profiles among the three groups. (B) Volcano plot shows that most differentially expressed genes (DEGs) are upregulated after intracerebral hemorrhage (ICH). (C) Volcano plot shows that most DEGs are downregulated after NYKD treatment. (D) Venn diagram shows 294 overlapped DEGs and 150 overlapping protein-coding genes. (E) Function analysis by MetaScape shows that the overlapped protein-coding genes are enriched in the functional cluster of cell activation, extra cellular matrix (ECM) degradation and remodeling, and inflammation ($n = 5$). Medium: medium dose; PC: principal component; FC: fold change; ECM: extracellular matrix.

3.9. The effects of the ICH-tailored TCM prescription on glial cell activation and neuroinflammation

The functions of both the predicted targets and actual DEGs of NYKD were enriched in cell activation and neuroinflammation. Therefore, we examined two major ICH-activated inflammation-associated glial cells: astrocytes and microglia. Immunofluorescence showed that pre-hematoma astrocytes ($GFAP^+$) were activated (intense GFAP staining and cellular hypertrophy) and proliferated ($GFAP^+$ and $PCNA^+$) in the ICH mice (Figs. 7A and B). Similarly, microglia were activated and proliferated ($Iba1^+$ and $PCNA^+$) after ICH (Figs. 7C and D). In the NYKD group, the numbers of proliferating astrocytes and microglia were significantly lower than those in the ICH group (Figs. 7A–D). Moreover, pro-inflammatory microglia (M1, $Iba1^+$, and $CD86^+$) were markedly reduced after NYKD intervention (Figs. 7E and F), whereas anti-inflammatory and phagocytic microglia (M2, $Iba1^+$, and $Arg1^+$) tended to increase in the treated group (Figs. 7G and H).

4. Discussion

In this study, we established a multi-targets-oriented gradient targets-compound-herb weighting strategy. Using this strategy, we formulated a new TCM prescription (NYKD) for ICH treatment. The five-herb prescription not only contains the classically used ICH-curative herbs but also includes non-conventional but rational members. The combination of herbs in NYKD also meets the TCM theory. The *in vivo* study showed that NYKD achieved multiple tailored effects in ICH mice, which was consistent with the function of the potential targets of NYKD. Moreover, the efficacy of NYKD is equal to that of the classical formula, XFZYD, although the new formula consists of fewer herbs than those in XFZYD.

Traditionally, the symptom- and sign-based syndrome differentiation has been the core step in disease diagnosis and prescription formulation by traditional Chinese physicians. Although this method is effective in some cases, it has several limitations. First, the symptoms and signs may not specifically or precisely

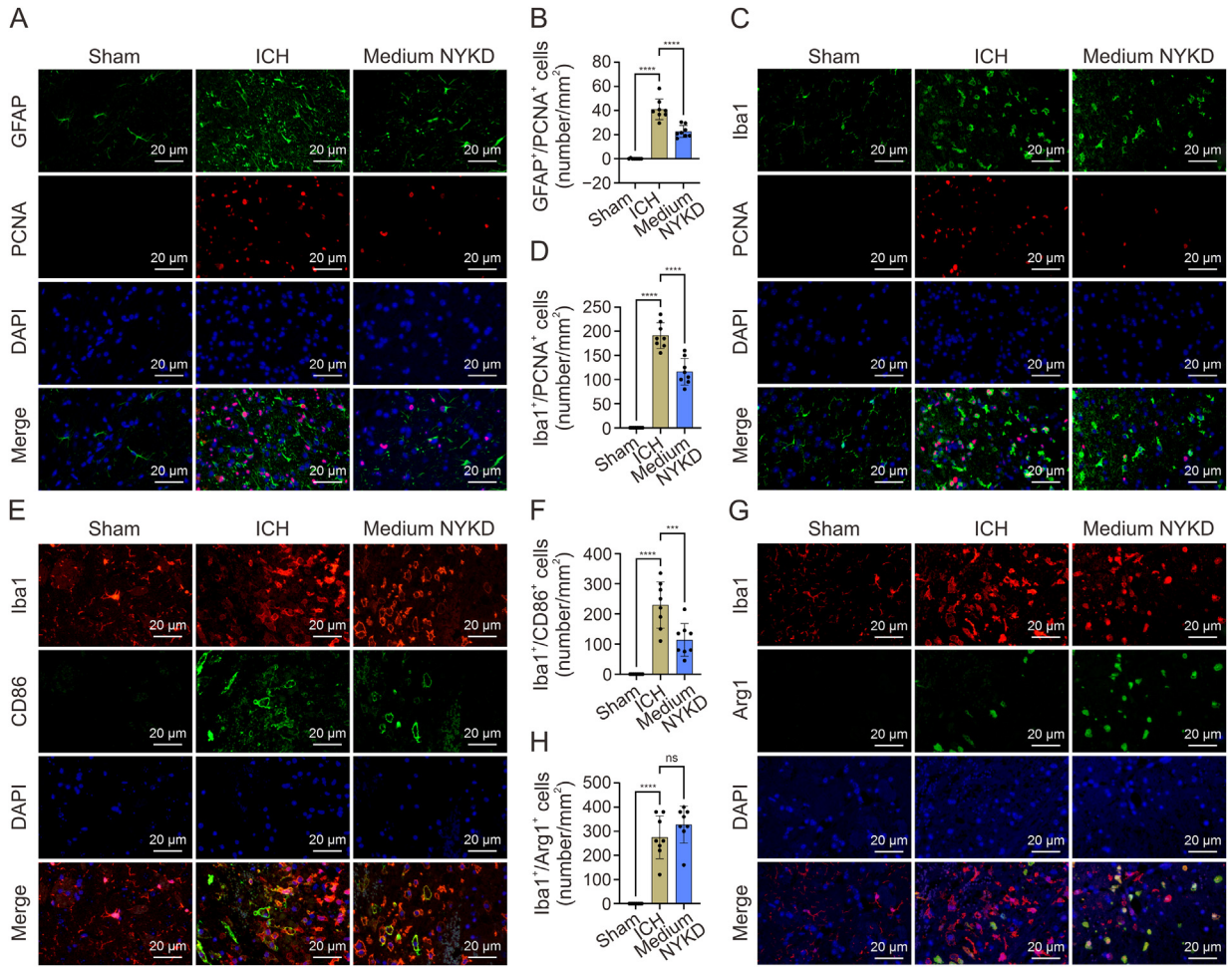

Fig. 7. Nao Yi Kang decoction (NYKD) inhibits glial cell activation and proliferation. (A, B) Immunofluorescent staining shows that NYKD inhibits astrocyte activation (green) and decreases the number of proliferating astrocytes: representative images of glial fibrillary acidic protein (GFAP) and proliferating cell nuclear antigen (PCNA) double staining (A) and statistic diagram of the number of double positive cells of GFAP and PCNA. (C, D) Immunofluorescent staining shows that NYKD inhibits microglia activation (green) and decreases the number of proliferating microglia: representative images of ionized calcium-binding adaptor molecule 1 (Iba1) and PCNA double staining (C) and statistic diagram of the number of double positive cells of Iba1 and PCNA (D). (E, F) Immunofluorescent staining shows that NYKD decreased the number of M1 microglia: representative images of Iba1 and cluster of differentiation 86 (CD86) double staining (E) and statistic diagram of the number of double positive cells of Iba1 and CD86 (F). (G, H) Immunofluorescent staining shows that NYKD increases the number of M2 microglia: representative images of Iba1 and arginase 1 (Arg1) double staining (G) and statistic diagram of the number of double positive cells of Iba1 and Arg1 (H). Data are presented as mean ± standard deviation (SD) ($n = 5$). $^{***}P < 0.001$ and $^{****}P < 0.0001$. ns: not significant. ICH: intracerebral hemorrhage; Medium: medium dose; DAPI: diamidino-phenyl-indole.

reflect the pathophysiology of the disease. Therefore, TCM diagnoses and prescriptions are relatively crude. Second, a selection bias exists with TCM combination therapy. The Chinese physician often formulates a prescription in reference to ancient records like “Treatise on Febrile Diseases” (Shang Han Lun) and “Synopsis of Prescriptions of theGolden Chamber” (Jingui Yaolüe). Although these classical prescriptions have been proven effective in clinical practice for thousands of years, the enrollment of TCM is limited owing to the limitations of the ancient perceptions, personal familiarity, and preference of locally distributed TCM. Recently, researchers applied the big data to analyze the law of TCM use in certain diseases and assist TCM formulation [4–6]. This strategy extends data coverage but cannot completely eliminate bias. Raw TCM prescriptions that input the statistics originate from personal clinical experiences. Our strategy uses an extensively covered target cluster instead of symptoms and signs to characterize a disease and applies a weighted disease-target-herbal ingredient-herb network to direct TCM formulation. This provides a relatively precise, multipronged, unbiased, and standardized approach for TCM formulations.

In our strategy, the reliability of the resulting formula largely relies on the relevance scores of the targets for ICH and the connections between the ingredients and targets. We obtained the relevance score of targets to ICH from GeneCards (the Human Gene Database) and the ingredient-target relations from SymMap. Both of them are comprehensive and authoritative databases that are widely used in network pharmacological research for TCM [21–23]. GeneCards integrates information from genomics, clinical trials, the literature, and more than 190 specialized databases [16]. It computes the relevance score of targets to diseases using the Elasticsearch 7.11 platform, which uses the well-recognized Boolean model to find matching documents and a practical scoring function to calculate the relevance. Because the source data are fuly covered, large-scale, and promptly updated, relevance scores in GeneCards database are relatively reliable [16]. SymMap is an integrative database specialized in TCM investigations [17]. Information about the compound-target interactions was integrated from two well-known databases: Hit 2.0 and TCMSP. Hit 2.0 collects the verified compound-target relationships from the literature [24]. TCMSP includes compound-target interactions from experimental validation and

predictive targets from the SysDT model, which have a concordance of 82.83%, sensitivity of 81.33%, and specificity of 93.62% [18]. Since its publication in 2019, SymMap has been cited more than 300 times [17]. Therefore, the component-target interactions are credible.

The basic TCM pathogenesis of ICH involves blood stasis (Yuxue) and toxic heat (Redu). *Hippophae rhamnoides* L. with *Ginkgo biloba* L. are utilized to promote the blood circulation and remove stasis (Huoxuehuayu), and *Scutellaria barbata* D. Don is used to clear heat and detoxification (Qingrejiedu). They are the monarchies because they address the principal underlying pathological mechanisms of ICH. Second, *Carthamus tinctorius* L. promotes the blood circulation (Huoxue), and *Achyranthes bidentata* Blume clears heat (Qingre), which assists the monarch. Therefore, they became ministers. Third, *Hippophae rhamnoides* L. is the assistant, because it promotes the blood circulation, protects the spleen and stomach, and prevents gastrointestinal complications after ICH and herb treatment (Huoxue and Jianpi). Last, *Achyranthes bidentata* Blume also clears heat and guides the stasis and heat toxins downward, which serves as the guide. Taken together, the function of NYKD is promoting "blood circulation and remove stasis" and "clearing heat and detoxification", which fully meets the primary pathophysiology of ICH.

Among the five herbs, *Achyranthes bidentata* Blume and *Carthamus tinctorius* L. are the most commonly used in ICH-treating TCM prescriptions, including XFZYD [20,25]. These results support the rationale of our TCM strategy. In contrast, *Hippophae rhamnoides* L., *Ginkgo biloba* L., and *Scutellaria barbata* D. Don are seldom included in traditional medicines. Previous research has indicated that *Hippophae rhamnoides* L. can reduce vascular leakage in the brain [26]; *Ginkgo biloba* L. and its active ingredients can inhibit apoptosis and improve the outcomes of patients with stroke [27–29]; and the extract of *Scutellaria barbata* D. Don protects against neuronal injuries and reduces glial cell expression [30–32]. This suggests that in addition to the classically used herbs, our strategy can underscore the therapeutic potential of non-canonical herbs.

In animal experiments, NYKD improved post-ICH neurological deficits through a multifactorial mechanism, including suppression of neuronal damage, cell apoptosis, and vascular leakage, reduction of hematoma volume, inhibition of astrocyte/microglia activation and proliferation, and limition of neuroinflammation. This indicates that this new strategy can be used to formulate effective TCM prescriptions for complex diseases. Although the effects of NYKD are almost equal but not superior to those of XFZYD in ICH mice, the number of herbs in NYKD is much lower than that in XFZYD. This indicates that NYKD may be a more convenient and less expensive treatment option for patients with ICH. Therefore, the NYKD is considered the optimal prescription [33].

The DEGs in the transcriptomics of NYKD-treated mice are less consistent with the potential targets from network prediction. Most herbal ingredients act by binding to target proteins and primarily alter downstream function rather than expression levels [34]. The function of NYKD validated by transcriptomics matches well with the predicted function of NYKD in our study, where both of them are enriched in the processes of cell activation and development, vascular damage and remodeling, and inflammation.

Blood coagulation and hematoma absorption are the major processes that after ICH outcomes [11]. First, rapid coagulation stops the expansion of the hematoma, decreasing mortality and potentially reducing brain injury [35]. In addition, the promoted absorption of the hematoma relieves secondary brain damage and potentiates neuronal repair [36,37]. TCM, classified as "Huoxuehuayu", may affect blood coagulation and resolution. The prescription highlighted in the present study belongs to this catalog. Although NYKD tended to increase the APTT and decrease the FIB levels, these changes were slight and insignificant. Moreover, the hematoma did not enlarge at the medium dose. This suggests that NYKD does not affect blood coagulation, and that it is safe to treat ICH with NYKD in the acute stage. In addition, NYKD substantially increased the number of phagocytic microglia (M2) and decreased hematoma volume. This implies that NYKD facilitates hematoma absorption.

Our study has several limitations. First, because the quantitative data about the amount of most ingredients in the herbs and the binding affinity of compounds to the targets are lacking, we did not integrate the intensity of herb-ingredient and ingredient-target interactions into the gradient weighting strategy, which unavoidably reduced the accuracy of the tailored prescription. Second, the efficacy of this strategy requires further validation in other diseases and models. Third, owing to the lack of highly credible databases that include the TCM syndrome-related targets, we did not apply this strategy to formulate TCM syndrome-specific prescriptions. Future studies will focus on establishing a disease- and syndrome-tailored TCM formulation platform to extend the application of our multi-target-based weighting strategy to complex diseases.

5. Conclusion

We proposed a multi-target-directed gradient weighting strategy to tailor disease-specific TCM prescriptions. Based on this strategy, we formulated a five-herb TCM prescription for ICH treatment. The new TCM formula also meets TCM theory and contains both well-recognized and less commonly used herbs. In animal models, tailored TCM prescriptions exert multifactorial effects on ICH. This novel strategy presents a promising avenue for formulating and optimizing a precise, multipronged, unbiased, standardized, and effective TCM prescription for complex diseases, particularly for physicians without sufficient systematic TCM knowledge. It provides a paradigm for modern achievements-driven standardization and innovation of TCM conception and will promote the modernization and globalization of TCM.

CRediT authorship contribution statement

Zhe Yu: Investigation, Data curation, Formal analysis, Writing – review & editing. **Teng Li:** Writing – review & editing, Visualization, Investigation, Funding acquisition. **Zhi Zheng:** Investigation. **Xiya Yang:** Investigation, Funding acquisition, Formal analysis. **Xin Guo:** Investigation. **Xindi Zhang:** Investigation. **Haoying Jiang:** Investigation. **Lin Zhu:** Funding acquisition, Formal analysis. **Bo Yang:** Funding acquisition, Formal analysis. **Yang Wang:** Supervision, Funding acquisition. **Jiekun Luo:** Writing – review & editing, Supervision. **Xueping Yang:** Writing – review & editing, Funding acquisition. **Tao Tang:** Writing – review & editing, Supervision, Funding acquisition, Data curation, Conceptualization. **En Hu:** Writing – review & editing, Writing – original draft, Supervision, Investigation, Funding acquisition, Data curation, Conceptualization.

Declaration of competing interest

We declare that we have no financial and personal relationships with other people or organizations that can inappropriately influence our work, and there is no professional or other personal interest of any nature or kind in any product, service and/or company that could be construed as influencing the position presented in our manuscript.

Acknowledgments

This work was supported by the National Natural Science Foundation of China (Grant Nos.: 82174259 and 82304997), China Postdoctoral Followship Program of CPSF (Grant No.: GZC20233202), China Postdoctoral Science Foundation (Grant No.:

2024M753698), the Key Research and Development Program of Hunan Province of China (Grant Nos.: 2023SK2021 and 2022SK2015), the Natural Science Foundation of Hunan Province, China (Grant Nos.: 2024JJ6632, 2022JJ40853, and 2021JJ31117), the Hunan Traditional Chinese Medicine Scientific Research Program, China (Grant Nos.: B2024113, B2024114, and 2021032), and the Fundamental Research Funds for the Central Universities of Central South University, China (Grant No.: 1053320232786). We thank Novogene Co., Ltd. for the RNA sequencing services, Biotree Biomedical Technology Co., Ltd. for compound detection, and the BioRender platform (https://www.biorender.com) for providing the icons used in Fig. 1.

Appendix A. Supplementary data

Supplementary data to this article can be found online at https://doi.org/10.1016/j.jpha.2025.101199.

References

[1] D. Pepe, M. Grassi, Investigating perturbed pathway modules from gene expression data via structural equation models, BMC Bioinformatics 15 (2014), 132.
[2] T.Y. Lo, A.S.L. Chan, S.T. Cheung, et al., Multi-target regulatory mechanism of Yang Xin Tang - a traditional Chinese medicine against dementia, Chin. Med. 18 (2023), 101.
[3] L. Wei, Z. Wang, N. Jing, et al., Frontier progress of the combination of modern medicine and traditional Chinese medicine in the treatment of hepatocellular carcinoma, Chin. Med. 17 (2022), 90.
[4] Y. Li, F. Zhang, H. Wang, et al., Screening and evaluation of core prescriptions for impotence based on network robustness and data mining, Zhongguo Zhong Yao Za Zhi 49 (2024) 4230–4237.
[5] J. Xiong, J. Wang, Y. Liu, et al., Study on prescription medication mode and mechanism of traditional Chinese medicine in the treatment of noncritical COVID-19 based on data mining, Tradit. Med. Res. 8 (2023), 36.
[6] W. Zhao, W. Lu, Z. Li, et al., TCM herbal prescription recommendation model based on multi-graph convolutional network, J. Ethnopharmacol. 297 (2022), 115109.
[7] M. Cheng, T. Li, E. Hu, et al., A novel strategy of integrating network pharmacology and transcriptome reveals antiapoptotic mechanisms of Buyang Huanwu Decoction in treating intracerebral hemorrhage, J. Ethnopharmacol. 319 (2024), 117123.
[8] X. Gan, Z. Shu, X. Wang, et al., Network medicine framework reveals generic herb-symptom effectiveness of traditional Chinese medicine, Sci. Adv. 9 (2023), eadh0215.
[9] Y. Cai, Z. Yu, X. Yang, et al., Integrative transcriptomic and network pharmacology analysis reveals the neuroprotective role of BYHWD through enhancing autophagy by inhibiting Ctsb in intracerebral hemorrhage mice, Chin. Med. 18 (2023), 150.
[10] G.E. Croston, The utility of target-based discovery, Expert Opin. Drug Discov. 12 (2017) 427–429.
[11] L. Puy, A.R. Parry-Jones, E.C. Sandset, et al., Intracerebral haemorrhage, Nat. Rev. Dis. Primers 9 (2023), 14.
[12] M. Selim, L.D. Foster, C.S. Moy, et al., Deferoxamine mesylate in patients with intracerebral haemorrhage (i-DEF): A multicentre, randomised, placebo-controlled, double-blind phase 2 trial, Lancet Neurol. 18 (2019) 428–438.
[13] C.S. Anderson, Reduction of iron neurotoxicity in intracerebral haemorrhage, Lancet Neurol. 18 (2019) 416–417.
[14] Q. Guo, S. Yang, D. Yang, et al., Differential mRNA expression combined with network pharmacology reveals network effects of Liangxue Tongyu Prescription for acute intracerebral hemorrhagic rats, J. Ethnopharmacol. 246 (2020), 112231.
[15] D. Xue, Z. Zhen, K. Wang, et al., Uncovering the potential mechanism of Xue Fu Zhu Yu Decoction in the treatment of intracerebral hemorrhage, BMC Complement. Med. Ther. 22 (2022), 103.
[16] M. Rebhan, V. Chalifa-Caspi, J. Prilusky, et al., GeneCards: Integrating information about genes, proteins and diseases, Trends Genet. 13 (1997), 163.
[17] Y. Wu, F. Zhang, K. Yang, et al., SymMap: An integrative database of traditional Chinese medicine enhanced by symptom mapping, Nucleic Acids Res. 47 (2019) D1110–D1117.
[18] J. Ru, P. Li, J. Wang, et al., TCMSP: A database of systems pharmacology for drug discovery from herbal medicines, J. Cheminform. 6 (2014), 13.
[19] C.P. Commission, Pharmacopoeia of the People's Republic of China, 1st ed., Vol. 1, Medicine Science and Technology Press of China, Beijing, 2020, pp. 74–75, 122–123, 157–158, 191–192, 329–330.
[20] Z. Yang, Y. Wu, X. Li, et al., Bioinformatics analysis of miRNAs and mRNAs network-Xuefu Zhuyu decoction exerts neuroprotection of traumatic brain injury mice in the subacute phase, Front. Pharmacol. 13 (2022), 772680.
[21] J. Yu, S. Wang, J. Yang, et al., Exploring the mechanisms of action of Zengye decoction (ZYD) against Sjogren's syndrome (SS) using network pharmacology and animal experiment, Pharm. Biol. 61 (2023) 1286–1297.
[22] T. Chen, S. Li, D. Lian, et al., Integrated network pharmacology and experimental approach to investigate the protective effect of Jin gu Lian capsule on rheumatoid arthritis by inhibiting inflammation via IL-17/NF-κB pathway, Drug Des. Devel. Ther. 17 (2023) 3723–3748.
[23] B. Yu, M. Zhou, Z. Dong, et al., Integrating network pharmacology and experimental validation to decipher the mechanism of the Chinese herbal prescription modified Shen-Yan-Fang-Shuai formula in treating diabetic nephropathy, Pharm. Biol. 61 (2023) 1222–1233.
[24] D. Yan, G. Zheng, C. Wang, et al., HIT 2.0: An enhanced platform for Herbal Ingredients' Targets, Nucleic Acids Res. 50 (2022) D1238–D1243.
[25] T. Duan, L. Li, Y. Yu, et al., Traditional Chinese medicine use in the pathophysiological processes of intracerebral hemorrhage and comparison with conventional therapy, Pharmacol. Res. 179 (2022), 106200.
[26] J. Purushothaman, G. Suryakumar, D. Shukla, et al., Modulatory effects of seabuckthorn (*Hippophae rhamnoides* L.) in hypobaric hypoxia induced cerebral vascular injury, Brain Res. Bull. 77 (2008) 246–252.
[27] Y. Hu, M. Huang, X. Dong, et al., Ginkgolide B reduces neuronal cell apoptosis in the hemorrhagic rat brain: Possible involvement of Toll-like receptor 4/nuclear factor-kappa B pathway, J. Ethnopharmacol. 137 (2011) 1462–1468.
[28] Z. Li, G. Xiao, H. Wang, et al., A preparation of *Ginkgo biloba* L. leaves extract inhibits the apoptosis of hippocampal neurons in post-stroke mice via regulating the expression of Bax/Bcl-2 and caspase-3, J. Ethnopharmacol. 280 (2021), 114481.
[29] T. Meng, Y. You, M. Li, et al., Chinese herbal medicine *Ginkgo biloba* L. preparations for ischemic stroke: An overview of systematic reviews and meta-analyses, J. Integr. Med. 22 (2024) 163–179.
[30] J. Cheng, Q. Guo, X. Wu, et al., *Scutellaria barbata* flavonoids improve the composited aβ-induced abnormal changes in glial cells of the brains of rats, Comb. Chem. High Throughput Screen. 25 (2022) 64–76.
[31] S.R. Lee, M.S. Kim, S. Kim, et al., Constituents from *Scutellaria barbata* inhibiting nitric oxide production in LPS-stimulated microglial cells, Chem. Biodivers. 14 (2017), e1700231.
[32] X.G. Wu, S.S. Wang, H. Miao, et al., *Scutellaria barbata* flavonoids alleviate memory deficits and neuronal injuries induced by composited Aβ in rats, Behav. Brain Funct. 12 (2016), 33.
[33] Z. Zhen, D. Xue, Y. Chen, et al., Decoding the underlying mechanisms of Di-Tan-Decoction in treating intracerebral hemorrhage based on network pharmacology, BMC Complement. Med. Ther. 23 (2023), 44.
[34] Y. Mao, J. Sun, Z. Wang, et al., Combining transcriptomic analysis and network pharmacology to explore the mechanism by which Shaofu Zhuyu decoction improves diabetes mellitus erectile dysfunction, Phytomedicine 119 (2023), 155006.
[35] D.J. Gladstone, R.I. Aviv, A.M. Demchuk, et al., Effect of recombinant activated coagulation factor VII on hemorrhage expansion among patients with spot sign-positive acute intracerebral hemorrhage: The SPOTLIGHT and STOP-IT randomized clinical trials, JAMA Neurol 76 (2019) 1493–1501.
[36] X. Lan, X. Han, Q. Li, et al., Modulators of microglial activation and polarization after intracerebral haemorrhage, Nat. Rev. Neurol. 13 (2017) 420–433.
[37] G. Wang, L. Wang, X. Sun, et al., Haematoma scavenging in intracerebral haemorrhage: From mechanisms to the clinic, J. Cell. Mol. Med. 22 (2018) 768–777.